Processing and Application of Ceramics 15 [3] (2021) 256–269
https://doi.org/10.2298/PAC2103256D

Magnetoelectric properties of materials based on barium zirconium titanate and various magnetic compounds

Adis S. Dzunuzovic*, Mirjana M. Vijatovic Petrovic, Jelena D. Bobic, Nikola I. Ilic, Biljana D. Stojanovic

Institute for Multidisciplinary Research, University of Belgrade, Belgrade, Serbia

Received 25 March 2021; Received in revised form 8 July 2021; Accepted 11 August 2021

Abstract

Multiferroic composites containing ferroelectric $Ba(Ti_{0.80}Zr_{0.20})O_3$ (BT80Zr20) phase and magnetic $Ni_{0.7}Zn_{0.3}Fe_2O_4$ (NZF), $CoFe_2O_4$ (CF) or $Ni_{0.7}Cu_{0.01}Sm_{0.05}Zn_{0.29}Fe_{1.95}O_4$ (NCuSmZF) phase were investigated in this study. Three composites, BT80Zr20-NZF, BT80Zr20-CF and BT80Zr20-NCuSmZF were prepared by mixing chemically synthesized powders in the planetary mill, uniaxial pressing and sintering at 1300 °C. X-ray diffraction data for the single phase and composites ceramics indicated the formation of crystallized structure of both ferrites and barium zirconium titanate, without the presence of undesirable phases. Microstructure analysis has shown the formation of two types of nanosized grains, polygonal ferromagnetic and rounded ferroelectric grains. Non-saturated hysteresis loops were evident in all composite samples possibly due to the presence of very high conductive ferrite phases. The BT80Zr20-CF has shown the lowest conductivity values in comparison with other two compounds and therefore the highest potential for ferroelectric application. The impedance investigations confirmed the presence of different relaxation processes that originate from the grain and grain boundary contributions. Investigation of J-E relation between leakage and electric field for the BT80Zr20 and composites revealed the presence of four possible mechanisms of conduction in these materials.

Keywords: *multiferroic composites, ceramics, magnetoelectric properties*

I. Introduction

Magnetoelectric multiferroics are advanced materials which possess wide area of application for sensors, storage, the emerging field of spintronics, electrically tunable microwave devices such as filters, multistate memory devices, oscillators and phase shifters [1,2]. These materials at the same time exhibit both magnetic and electric properties and, as such, attract a great deal of interest in research and application. Multiferroics are defined as materials having more than one ferroic properties (ferroelectric, ferromagnetic and ferroelastic) at the same time [3]. In recent years there has been increased interest in structures of lower dimensionality, such as thin films or complex composites including flexible structures. An important restriction in the fabrication of these materials is dictated by the need for the reduced cost and improved functionality of the system [4]. With their promising properties, multiferroic materials could likely offer new types of devices with great functionalities. Many researchers have developed processes and techniques to enhance the quality and reproducibility of powders and to produce multiferroic materials as single phase multiferroics ($BiFeO_3$, $BiMnO_3$) or in the form of composites ($(NiZn)Fe_2O_4$-$BaTiO_3$, $BaSrTiO_3$-Ni, $ZnFe_2O_4$, $Ni(Co,Mn)Fe_2O_4$-$BaTiO_3$). Due to the importance of multiferroics materials, the significant attention has been drawn to their preparation. Multiferroic composites in comparison to single phase multiferroics have some advantages concerning the synthesis. For example $BiFeO_3$, as one of the representatives of single phase multiferroics, is hardly synthesized without impurities [5,6].

The simplest way of composites preparation is mixing of pure ferroelectric and ferromagnetic powders in a desired mass ratio in a different type of mills. During the years, various preparation methods of single phase materials have been developed and presented in the literature [7–10]. It is also very important to notice that properties of the obtained powders are highly dependent

* Corresponding authors: tel: +381 11 2085 039,
e-mail: *a.dzunuz@hotmail.com*

on preparation procedure and selection of the adequate method is rather essential especially if they are further used for the preparation of composites. These composite materials contain two different crystallographic phases, ferroelectric-perovskite and magnetic-spinel structure, with specific properties. When they are combined together in the composites, the properties (especially resistivity, dielectric constant, ferroelectric and magnetic properties) drastically change. Different relaxation processes that appear at the grain and grain boundary regions make it hard to determine the real impact of each phase present in the composite and to understand the processes and phenomena that occur in these types of materials. Nowadays multiferroic composites are among the most attractive multifunctional materials and it is challenging to prepare them in the equilibrium of ferroelectric and magnetic structures.

Our interest has been directed towards multiferroic composites based on $Ba(Ti_{0.80}Zr_{0.20})O_3$ (BT80Zr20) as ferroelectric phase and $Ni_{0.7}Zn_{0.3}Fe_2O_4$ (NZF), $CoFe_2O_4$ (CF), $Ni_{0.7}Cu_{0.01}Sm_{0.05}Zn_{0.29}Fe_{1.95}O_4$ (NCuSmZF) as ferromagnetic phases. These systems were developed according to previous studies of the authors that were based on $BaTiO_3$, $PbZr_{0.52}Ti_{0.48}O_3$ (as ferroelectric phases) and $NiZnFe_2O_4$, $CoFe_2O_4$ (as ferromagnetic phases) in different combinations [9,11–13]. $BaTiO_3$ (BT) possesses high permittivity, low dielectric loss and high tunability and it is widely used due to its specific ferroelectric and piezoelectric properties, [14,15]. At high temperatures, BT is stable in the paraelectric cubic phase and with decreasing temperatures phase transformation into ferroelectric phases occurs with tetragonal symmetry at T_{C-T} = 120 °C, orthorhombic at T_{T-O} = 5 °C and rhombohedral symmetry at −90 °C. The influence of various additives on structural, optical and electrical properties has also been reported previously [16,17]. There is a great interest to improve dielectric properties by doping with different dopants, such as La^{3+}, Mn^{3+}, Zr^{4+}, Hf^{4+}, Nb^{5+}. When Zr^{3+} is added in the $BaTiO_3$, the material retains classical ferroelectric behaviour and all three dielectric anomalies characteristic for BT are present in the material with enhanced dielectric and piezoelectric properties [18,19]. Selected ferrites for this study were ferromagnetic materials: NZF, CF and NCuSmZF. NZF as a good soft magnetic and CF as a semi-hard magnetic possess good electrostrictive properties, high electrical resistivity, high value of magnetization and high chemical stability [20,21]. Many reports are available in the literature for Cu-substituted NZF and Sm-substituted NZF. Pissurlekar [22] reported that in $Ni_{0.55-x}Cu_xZn_{0.45}Fe_2O_4$ (x = 0.0–0.15) saturation magnetization decreases as Cu concentration increases and hysteresis losses and coercivity are found to increase. Batoo *et al.* [23] synthesized nanoparticles of polycrystalline $Ni_{0.7-x}Cu_{0.3}Fe_2Zn_xO_4$ by auto-combustion method where the dielectric and AC conductivity parameters show their maximum value for 10% Zn-doping composition. Also, *Li et al.* [24] reported that increase of Cu in $Ni_{0.4-x}Zn_{0.6}Cu_xFe_2O_4$ decreases the lattice parameter and M_c and increases H_c. On the other hand, the addition of carefully defined amount of samarium in nickel zinc ferrite enables the control over the magnetic parameters [25], so saturation magnetization and coercive force increase with the increase in Sm content which is very useful for the application of the ferrite materials in the antenna construction [26].

The aim of this study was to prepare multiferroic composites with formula BT80Zr20-NZF/CF/NCuSmZF from nanopowders obtained by the auto-combustion method. The investigations of structural, electric and ferroelectric properties of these materials are reported and compared to available literature data.

II. Experimental

The raw materials used for the synthesis of NCuSmZF were $Fe(NO_3)_3 \cdot 9\,H_2O$ (Alfa Aesar, 98.0–101.0%), $Ni(NO_3)_2 \cdot 6\,H_2O$ (Alfa Aesar, 99.9985%), $Zn(NO_3)_2 \cdot 6\,H_2O$ (Alfa Aesar, 99%), $Sm(NO_3)_2 \cdot 6\,H_2O$ (Alfa Aesar, 99.9%), $Cu(NO_3)_2 \cdot 3\,H_2O$, $C_6H_8O_7 \cdot H_2O$ (Carlo Erba, 99.5–100.5%) and NH_4OH (Lach Ner, 25%). Metal nitrates and citric acid solution were mixed and pH value of the solution was adjusted to 7 with the ammonia solution. After the process of self-propagation reaction and thermal treatment at 1000 °C, the pure ferrite phase was obtained. NZF and CF were also synthesized with a process used for the NCuSmZF.

Starting reagents used for auto-combustion synthesis of $Ba(Ti_{0.8}Zr_{0.2})O_3$ were: $Ti(OCH(CH_3)_2)_4$ (TTIP) (Alfa Aesar, 98.0–101.0%), $C_6H_8O_7 \cdot H_2O$ (Carlo Erba, 99.5–100.5%), $Ba(NO_3)_2$, $Zr(O(NO_3)_2) \cdot 6\,H_2O$ (Alfa Aesar, 99.9%) and NH_4OH (Lach Ner, 25%). After self-propagation reaction, the precursor powder of BT80Zr20 was further calcined at 900 °C for 2 h.

Multiferroic composites with formula BT80Zr20-NZF/CF/NCuSmZF were obtained by mixing powder of obtained ferroelectric (BT80Zr20) and ferromagnetic phases (NZF, CF, NCuSmZF) in a planetary ball mill for 24 h. The synthesis routes for ferroelectric and ferromagnetic phases and composites were schematically presented in Fig. 1. Zirconia balls and isopropyl alcohol were used as a milling media. According to the previous reports, the mass ratio of ferroelectric and ferromagnetic phase was fixed to 80:20, respectively, for all compositions. The powders were pressed into circular discs with diameter of 8 mm using an uniaxial press at 195 MPa and the optimization of sintering process was carefully performed. Green compacts of the composites were sintered in the air atmosphere at 1300 °C for 4 h with natural cooling cycle.

The phase and crystalline structure of the single phase materials as well as composites were investigated

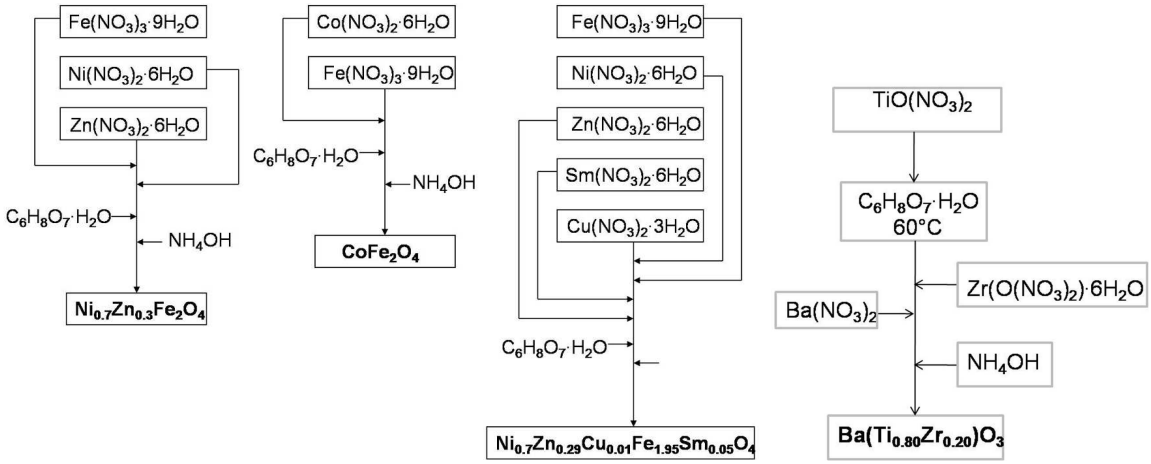

Figure 1. Scheme of barium zirconium titanate and ferrites preparation

by X-ray diffractometer (Model Rigaku RINT 2000, CuKα radiation). The microstructural characterization of the ceramics and the average grain size determination were done by scanning electron microscope (SEM-Model TESCAN SM-300). Impedance spectroscopy of the sintered pellets was performed in the frequency range from 42 Hz to 1 MHz and in the temperature range from 300 to 600 °C using an LCR meter (model 9593-01, HIOKI HITESTER). For electrical measurements silver electrodes were applied on both surfaces of the polished sintered ceramic samples. The experimental results were fitted using the commercial software package *ZView* and specific resistivity results were obtained and presented in detailed analysis.

III. Results and discussion

Besides composites, sintered samples of pure ferroelectric and ferromagnetic phases were prepared and used for the comparison of properties with appropriate composite pair. Figure 2a represents X-ray diffraction measurements for all specimens. The presence of the cubic spinel structures of NZF, NCuSmZF (according to JCPDS card No. 10-0325) and CF (according to JCPDS card No. 22-1086) as well as the formation of perovskite tetragonal phase of BT80Zr20 (according to JCPDS card No. 05-0626) can be observed. For the NCuSmZF sample some amount of $CuFe_2O_4$ phase is present (peak at 39°). Phase analysis of the composites is presented in Fig. 2b, and it points to the existence of the most prominent peaks of the tetragonal phase of BT80Zr20 at 32.5° and of the cubic ferrite phases that are located at 41.3° for NZF, 41.7° for CF and 42.3° for NCuSmZF. The formation of the pure BT80Zr20 phase reveals that added Zr ions in the BT structure completely exchange Ti-ions in the structure even though it possess higher ionic radius (Zr^{4+} (0.084 nm) compared to Ti^{4+} (0.061 nm)) [27,28]. From X-ray diffractograms of the obtained composites the presence of NZF, CF, NCuSmZF and BT80Zr20 phases without the presence of any intermediate phases or impurities can be confirmed. Powders of the composite materials were pressed at 195 MPa into pellets and sintered under the same sintering conditions: 4 h at the temperature of 1300 °C and the sintering rate of 5 °C/min. The density values were found to be 85.4, 92.8 and 88.6% TD (of the theoretical value) for the BT80Zr20-NZF, BT80Zr20-CF and BT80Zr20-NCuSmZF, respectively.

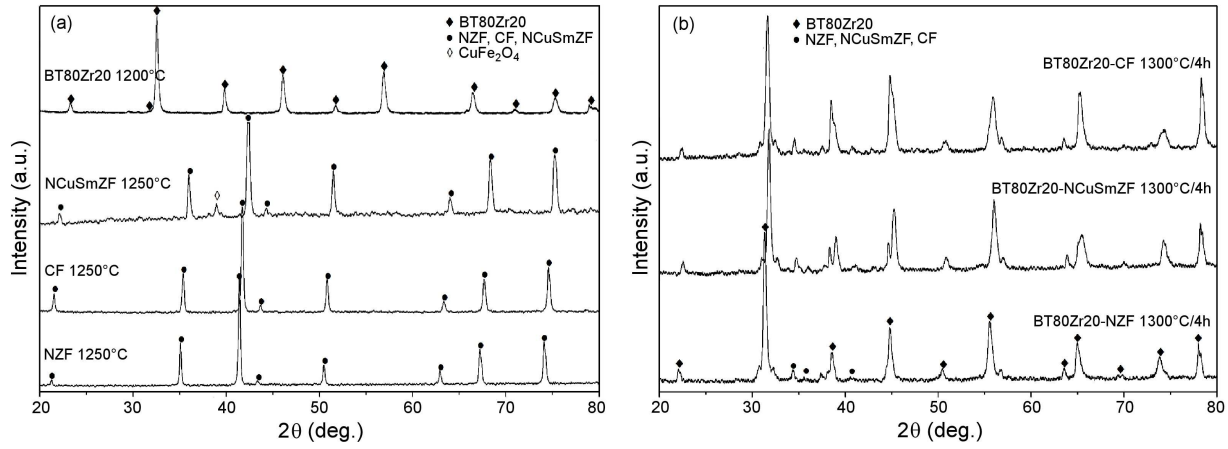

Figure 2. XRD difratograms of: a) BT80Zr20, NCuSmZF, CF, NZF and b) BT80Zr20-CF, BT80Zr20-NCuSmZF, BT80Zr20-NZF ceramics

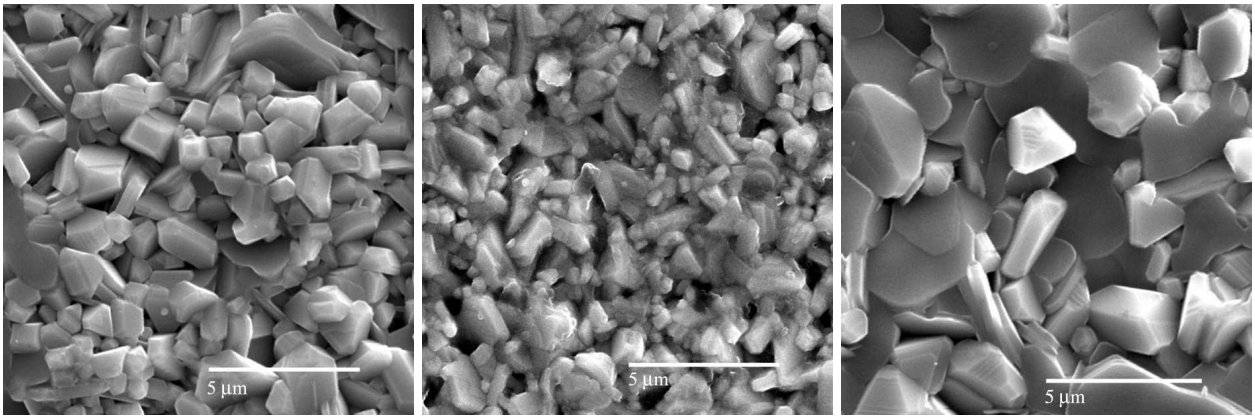

Figure 3. SEM images of: a) BT80Zr20-NZF, b) BT80Zr20-CF and c) BT80Zr20-NCuSmZF ceramics

SEM images of the obtained composites at the free surface are given in Fig. 3. Since the functional properties are expected to be critically dependent on the microstructure for these multiphase composites it is very important to know the distribution of the constituent phases which are present in the microstructures. Two types of grains are present in these samples: polygonal ferrite grains and more rounded grains of barium zirconium titanate. For the BT80Zr20-NZF and BT80Zr20-CF samples the average grain sizes are 0.83 and 0.71 µm respectively, and above 1 µm for the BT80Zr20-NCuSmZF. The sample with the smallest average grains size possesses the highest value of density (BT80Zr20-CF) and the lowest density was obtained for the sample BT80Zr20-NZF. Even though the sample BT80Zr20-NCuSmZF has the largest grains, the densification was improved possibly due to the presence of Cu^{2+} ions in octahedral sites of $NiCuSmZnFe_2O_4$ which led to a better density of this material compared to the one with NZF phase [29,30].

Complex impedance spectra (Nyquist plots) for all investigated ceramic composites at different temperatures are presented in Fig. 4. The temperature range for impedance measurements was from 300 to 400 °C for all composites and at higher temperatures 500–600 °C for the BT80Zr20 due to very high resistivity of this material that limited the analysis in the temperature region below 500 °C. The value of the grain, grain boundary and total electrical resistivity, obtained from the calculations using *ZView* software with equivalent circuits consisted of two or three parallel *R-CPE* elements connected in series, are presented in the Table 1. Cole-Cole plots for the pure ferroelectric phase have shown one depressed semicircular arc, indicating that the contributions of grain and grain boundary are overlapping. On the other hand, in the case of the composite samples, the presence of two semicircular arcs is evident, clearly separating the contribution that originates from the grain interior and from grain boundaries. Also, in the composites materials the look of the spectra can be influenced by various relaxation processes in different crystallographic phases. This analysis determined the presence of two semicircular arcs for the BT80Zr20-NZF and BT80Zr20-CF. The first one is due to the influence of the grain boundary conduction and the second one is due to the influence of grain conduction. For the sample BT80Zr20-NCuSmZF the best fitting parameters with the lowest fitting errors were obtained using three parallel *R-CPE* elements connected in series. In this case the third semicircular arc which was observed corresponds to the influence of electrode. The temperature range of measurements for the pure BT80Zr20 was from 500 to 600 °C, which is far above the Curie temperature due to very high resistivity of this material in the wide temperature region, while for composites the temperature range of measurements was from 300 to 400 °C. According to the results presented in Table 1, for all investigated composite samples total resistivities decrease with increasing temperature, which indicates the semiconducting nature and negative temperature coefficient of resistance. Impedance analysis of the BT80Zr20 sam-

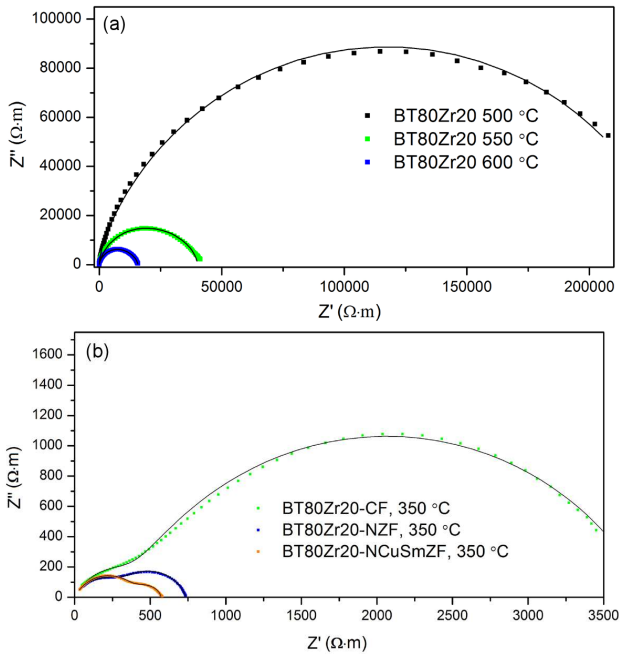

Figure 4. Impedance measurements for: a) BT80Zr20, b) BT80Zr20-NZF, BT80Zr20-CF, BT80Zr20-NCuSmZF at different temperatures

Table 1. Grain resistance, grain boundary resistance, total resistance and capacitance for measured samples

Sample	T [°C]	From Z''-Z'			From Z''-f
		R_g [Ω·m]	R_{gb} [Ω·m]	R_{total} [Ω·m]	C_{gb} [nF/m]
BT80Zr20	500	238400	1950	240350	4.54
	525	150900	1630	152530	4.03
	550	39450	1200	40150	3.28
	575	17100	4000	21000	2.85
	600	13250	2500	15750	2.72
BT80Zr20-NZF	300	490	590	1080	73.4
	325	430	440	870	66.8
	350	410	320	730	60.6
	375	390	250	640	56.1
	400	350	190	540	52.2
BT80Zr20-CF	300	890	17800	18690	146.5
	325	640	9090	9730	143.3
	350	330	3450	3780	142.1
	375	190	1590	1780	138.1
	400	110	760	870	133.1
BT80Zr20-NCuSmZF	300	380	1330	1710	9.45
	325	240	900	1140	8.62
	350	150	420	570	7.63
	375	100	290	390	6.56
	400	70	170	240	6.19

ple confirmed that these curves show the phenomena of decentralization where the value of the angle with x-axis increases with temperature increase. While the resistance of the BT80Zr20 is quite large, the resistance values for the composites are significantly lower compared to the values for pure ferroelectric phase which indicates a large influence of the magnetic phase on the impedance properties due to the higher conductivity of ferrite phase. In the ferrites, hopping of the Fe^{2+} and Fe^{3+} is responsible for conduction in the higher frequency region, while this hopping process at lower frequency region (grain boundary conduction is dominant) is ineffective. In addition to this in composites, the hopping of $3d$ electrons from Ti^{4+} to Ti^{3+} is also highly possible. In composites, the highest resistivity was found for the BT80Zr20-CF ceramics, for all temperatures. The samples BT80Zr20-CF and BT80Zr20-NCuSmZF have R_{gb} values which were higher in comparison with obtained respective values for R_g while the BT80Zr20 has higher value of R_g in comparison with obtained value for R_{gb}. Pure BTZr ferroelectric phase have shown dominant grain contribution in the total resistivity of the ceramics, in contrast to the composites BT80Zr20-CF and BT80Zr20-NCuSmZF, in which grain boundary resistivities had much higher values.

The BT80Zr20-CF has the smallest grains compared to other composites, which indicates the existence of a large number of grain boundaries. Because of that this composite shows the largest difference between resistance of grain and grain boundary. The BT80Zr20-NZF below 350 °C possesses higher value of R_{gb} and above 350 °C the grain effect can be ascribed as the dominant effect in total conduction. As expected, the sample BT80Zr20, as an ferroelectric phase, possesses higher value of resistivity in comparison with the composites samples due to the higher conductivity of ferrites phase.

Figure 5 shows the variation of conductivity with temperature for grains and grain boundaries for all the investigated samples. The temperature dependence of the resistance was given by the equation:

$$\sigma = \sigma_0 \cdot \exp\left(-\frac{E_a}{k_b \cdot T}\right) \tag{1}$$

where σ_0, E_a and k_b represent pre-exponential factor, activation energy and the Boltzmann constant, respectively. From the slope of these diagrams the activation energies can be obtained. For the composites BT80Zr20-NZF, BT80Zr20-CF and BT80Zr20-NCuSmZF the activation energies for the conduction process through grain boundaries have higher values in comparison with grains, while for the BT80Zr20 it is the reverse case. This phenomenon indicates higher impact of grain boundaries on the total resistivity for the composites samples. The value of activation energy for the BT80Zr20 is significantly higher compared to the values for composites. Usually, in the materials there are two types of conduction: i) electron hopping conduction where the needed activation energy is less than 0.7 eV and ii) above 0.7 eV which corresponds to the mobility of the defects in the crystal lattice. In the case of electron hopping conduction, activation energy is less than 0.2 eV for n-type polaronic conduction and above 0.2 eV for polaronic conduction of the holes [31]. Since these values for the pure BT80Zr20 for activation energy of both grain and grain boundary are above 0.7 eV, it may correspond to the motion of defects in the crystal lattice and here possibly can be attributed to the oxygen

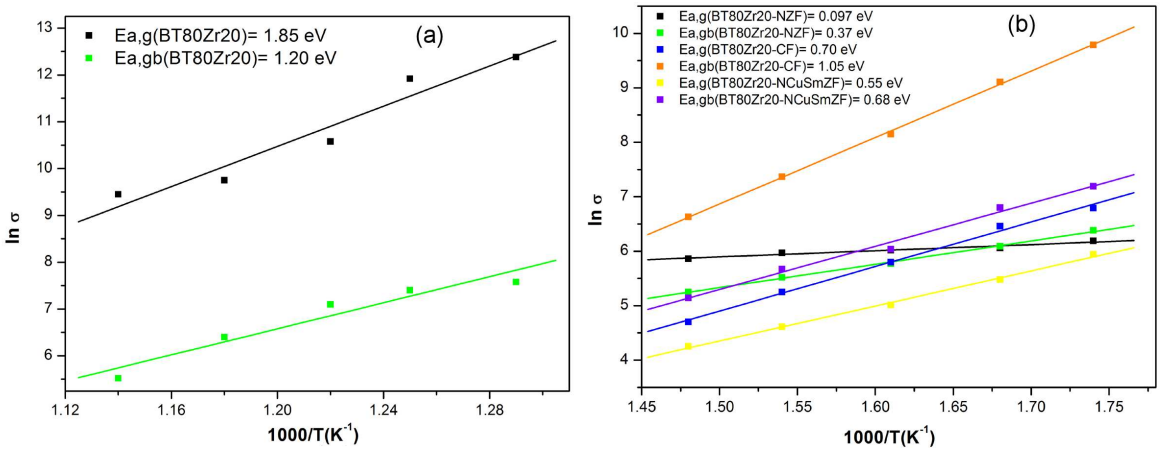

Figure 5. The Arrhenius plots of grain and grain boundary conductivity for: a) BT80Zr20, b) BT80Zr20-NZF, BT80Zr20-CF, BT80Zr20-NCuSmZF

vacancies motion, as reported in the literature [32,33]. In order to compensate the creation of oxygen vacancies, electrons and holes can be generated, which should further cause two different resistance responses. In these systems, an important role in the conduction process has hopping of 3*d* electrons. These phenomena can occur among Fe^{2+} and Fe^{3+}, Ni^{2+} and Ni^{3+} in ferrites as well as between Ti^{4+} and Ti^{3+} in perovskite lattice of barium zirconium titanate, in that way promoting the n-type conduction in the material. In the composites, the value of activation energy varies from low ~0.1 eV to relatively high ~1 eV. In the BT80Zr20-NZF, the activation energies were approximately 0.1 and 0.37 eV (for grain and grain boundary conduction) which can suggest the mechanism of polaronic conduction of both types. For the BT80Zr20-NCuSmZF the value of activation energy rises up to 0.68 eV. The reason for this may be the presence of Sm and Cu in the ferrite phase, NCuSmZF. Specifically, in addition to the presence of Ni^{2+}/Ni^{3+} there are also Cu^{2+}/Cu^{+} which can give rise to p-type carriers, contributing to the net polarization. Samarium affects the replacement of iron in the lattice and with Ni^{2+} ions it limits the degree of Fe^{2+} to Fe^{3+} transfer and vice versa, which obstructs electron hopping and results in an increase in resistivity and activation energy in the BT80Zr20-NCuSmZF composites.

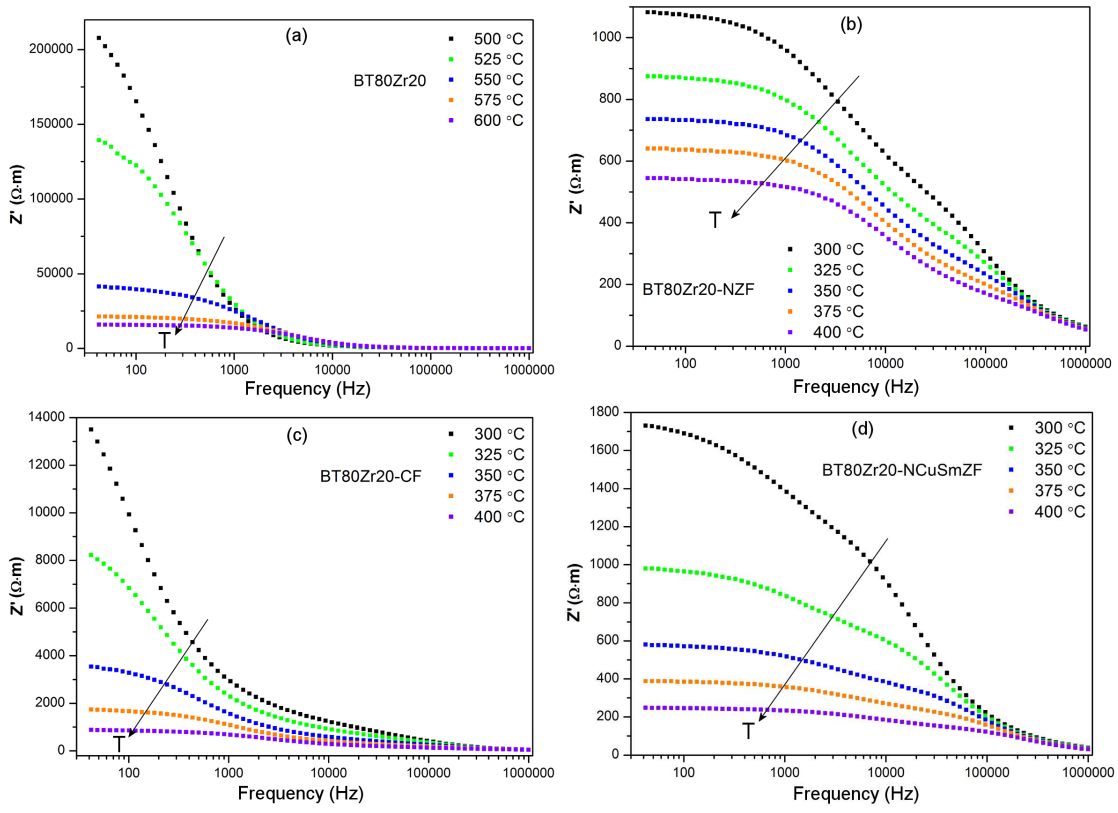

Figure 6. Variation of Z' with frequency at different temperatures for: a) BT80Zr20, b) BT80Zr20-NZF, c) BT80Zr20-CF and d) BT80Zr20-NCuSmZF ceramics

On the other hand, low value of activation energy in the BT80Zr20-NZF composites indicated more dominant hoping of electrons between Ti^{3+}/Ti^{4+} and Fe^{2+}/Fe^{3+} as well. From the obtained values for activation energy, the mobility of the defects in the crystal lattice of the BT80Zr20-CF may be considered as a type of conduction similar to the pure BT80Zr20 [34,35]. This shows that CF has the least effect on the activation energy in composites in comparison with NZF and NCuSmZF.

The variation of Z' of the pure BT80Zr20 and composites with frequency at different temperatures is shown in Fig. 6. For the BT80Zr20 and BT80Zr20-CF samples, the values of Z' are much higher in the low frequency region, followed by decreasing trend up to approximately 2 kHz. With further increase of frequency the value of Z' begins to decline by reaching a frequency independent plateau. In the samples BT80Zr20-NZF and BT80Zr20-NCuSmZF, different trend can be noticed, the value of Z' is constant in the low frequency region shifted to higher frequencies. At the end, these curves merge at 10 kHz for the BT80Zr20 and above 100 kHz for composites. The highest value of Z' at the low frequencies can be attributed to a slow dynamic relaxation process while merging of all curves into one single represent the release of space charge. In these materials a decrease in the value of Z' with an increase in temperature can be noticed which indicates the presence of negative temperature coefficient of resistance (NTCR) type behaviour in semiconductors.

The variation of the Z'' with frequency at different temperatures is shown in Fig. 7. The presence of one or two broad maxima is observed for all investigated samples. For different temperatures the value of Z'' had a maximum at different frequencies. With increasing temperature these peaks decrease toward the higher frequencies. This is an indication of existence of two possible phenomena: i) presence of the space charge polarization or accumulation at grain boundaries and ii) presence of the temperature dependent electrical relaxation in the material, due to the contribution of immobile parts at lower temperatures and mobile defects and vacancies in material at higher temperatures. Due to high temperature sintering process, traces of oxygen can be lost in ceramics grains while excess electrons and oxygen vacancies are formed in the following reduction reactions [36,37]:

$$O_O^x \longrightarrow \frac{1}{2} O_{2(g)} + V_O^x$$
$$V_O^x \longrightarrow V_O^{\cdot} + e^{\cdot}$$
$$V_O^{\cdot} \longrightarrow V_O^{\cdot\cdot} + 2\,e^{\cdot}$$
$$O_O^x \longrightarrow \frac{1}{2} O_{2(g)} + V_O^{\cdot\cdot} + 2\,e^{\cdot}$$

where all the species are written according to the Kröger-Vink notation of defects. These double charged oxygen vacancies are one of the most mobile charges in the perovskite ferroelectrics and play an important role in conduction processes in the material [38].

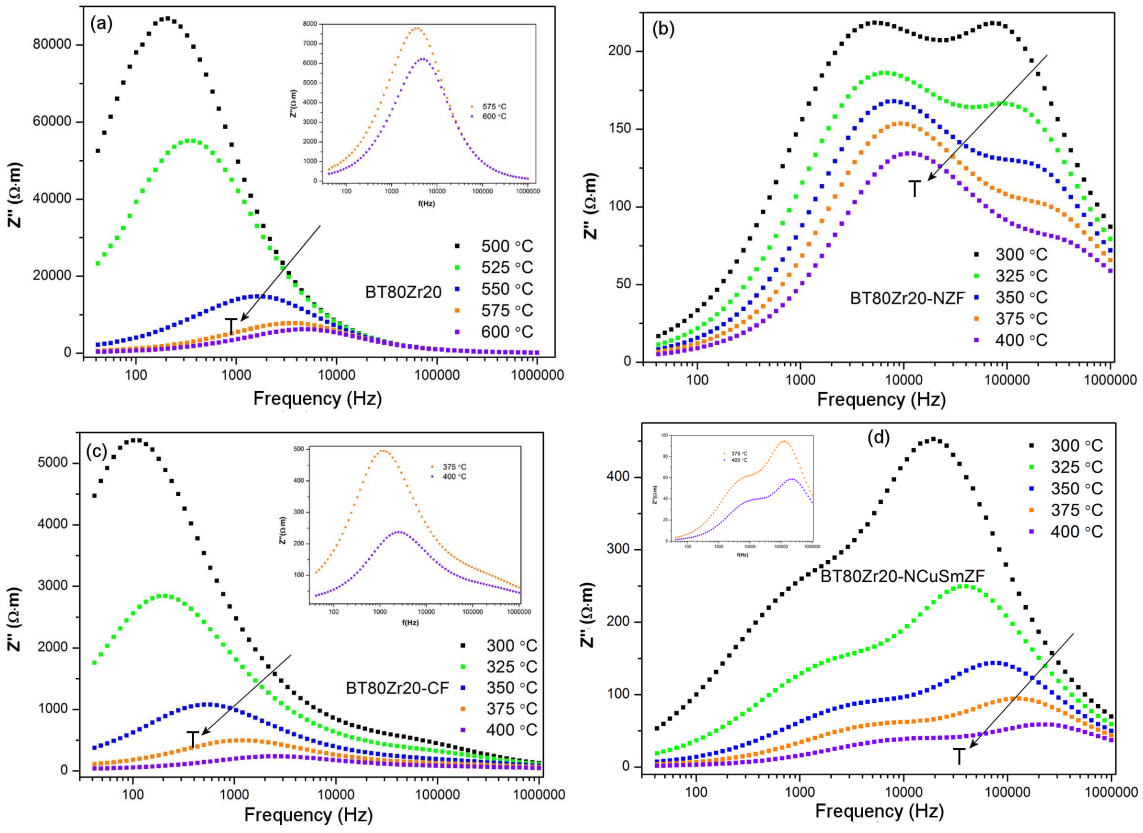

Figure 7. Imaginary parts of the impedance spectra as a function of frequency of: a) BT80Zr20, b) BT80Zr20-NZF, c) BT80Zr20-CF and d) BT80Zr20-NCuSmZF ceramics

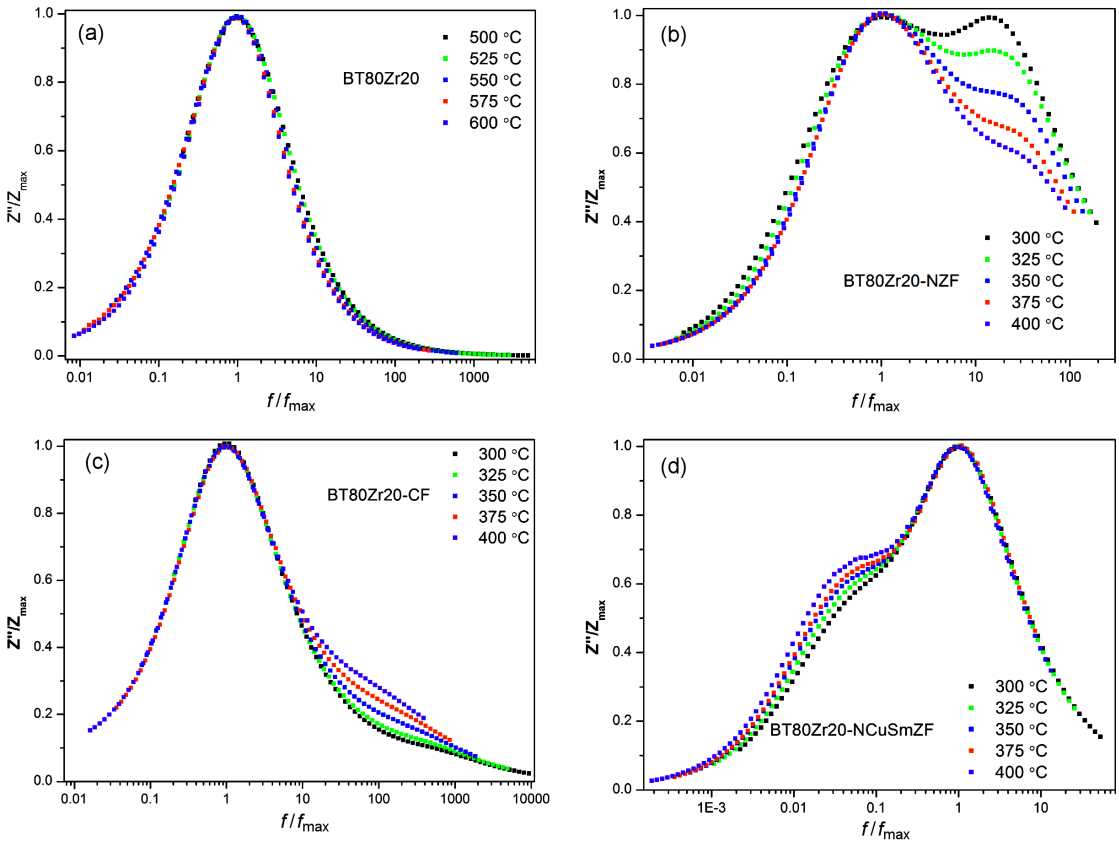

Figure 8. Frequency dependence Z''/Z_{max} of: a) BT80Zr20, b) BT80Zr20-NZF c), BT80Zr20-CF and d) BT80Zr20-NCuSmZF composites

On the other hand, the existence of different ferromagnetic phases in composites affected also the shape of these curves and broadening of these peaks indicated also the presence of phase dependent relaxation process in the investigated composites. Only for the BT80Zr20 the curves merge in the high frequency domain which indicates disappearance of the charge polarization. For the composites, curves merging is not present or it is present at much higher frequencies. The curves for the BT80Zr20 and BT80Zr20-CF possess one well noticeable maximum in the low frequency region, showing very similar behaviour (Fig. 7a,c). The other two compounds, BT80Zr20-NZF and BT80Zr20-NCuSmZF, besides the peak at low frequencies possess one broad maximum at higher frequencies as well (Fig. 7b,d). The peaks at lower frequencies are usually attributed to the relaxation mechanism associated with grain boundaries while the peaks at higher frequencies are related mainly to the grain contribution. From the values of Z''_{max} and fmax from the diagram, the values of capacitance are calculated according to the relationships $C = 1/2\pi \cdot f_{max} \cdot R$, where $R = 2 \cdot Z''_{max}$. The obtained values are presented in Table 1. The calculated values of capacitance for all the investigated samples decrease with the increase of temperature.

The scaling behaviour was studied using normalized parameters Z''/Z_{max} as a function of f/f_{max} for all the investigated samples (Fig. 8). For the BT80Zr20 it can be noticed that all data collapse into a single master curve for the whole frequency range, which indicates that the contribution of relaxation time is temperature independent. For the composites BT80Zr20-NZF and BT80Zr20-CF, the curves overlap nicely at lower frequencies while for the BT80Zr20-NCuSmZF the curves overlap at higher frequencies. At other frequencies the second broad peak appearance indicates the transition from long-range to short range mobility and temperature dependent relaxation time [39].

In order to determine different electro-active regions in the modulus and dynamical aspects of electrical transport phenomena, the frequency dependence of the imaginary part of modulus at different temperatures was investigated and presented in Fig. 9. For the pure BT80Zr20 two clear peaks can be observed, one in the low frequencies region, which indicates the contribution of grain boundaries to the conduction process in the material, and the other one in the high frequencies region which indicates the contribution of grains to the conduction process in the material. The increase of temperature leads to the shift of both peaks towards higher frequencies, indicating the hopping conduction mechanism of charge carriers and thermally activated dielectric relaxation in the material [40]. For the BT80Zr20-CF one peak can be observed at higher frequencies indicating the contribution of grains to the conduction process and the short range movement of charged particles. It was

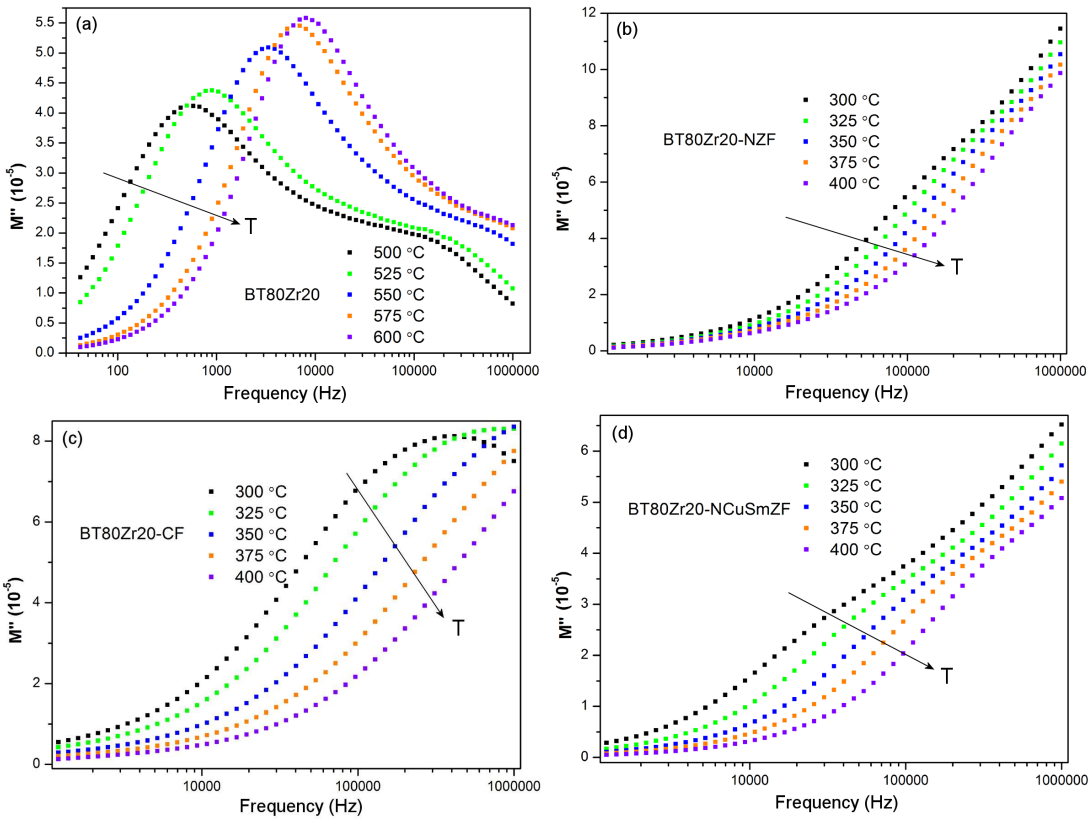

Figure 9. Imaginary parts of the impedance spectra as a function of frequency of: a) BT80Zr20, b) BT80Zr20-NZF, c) BT80Zr20-CF and d) BT80Zr20-NCuSmZF ceramics

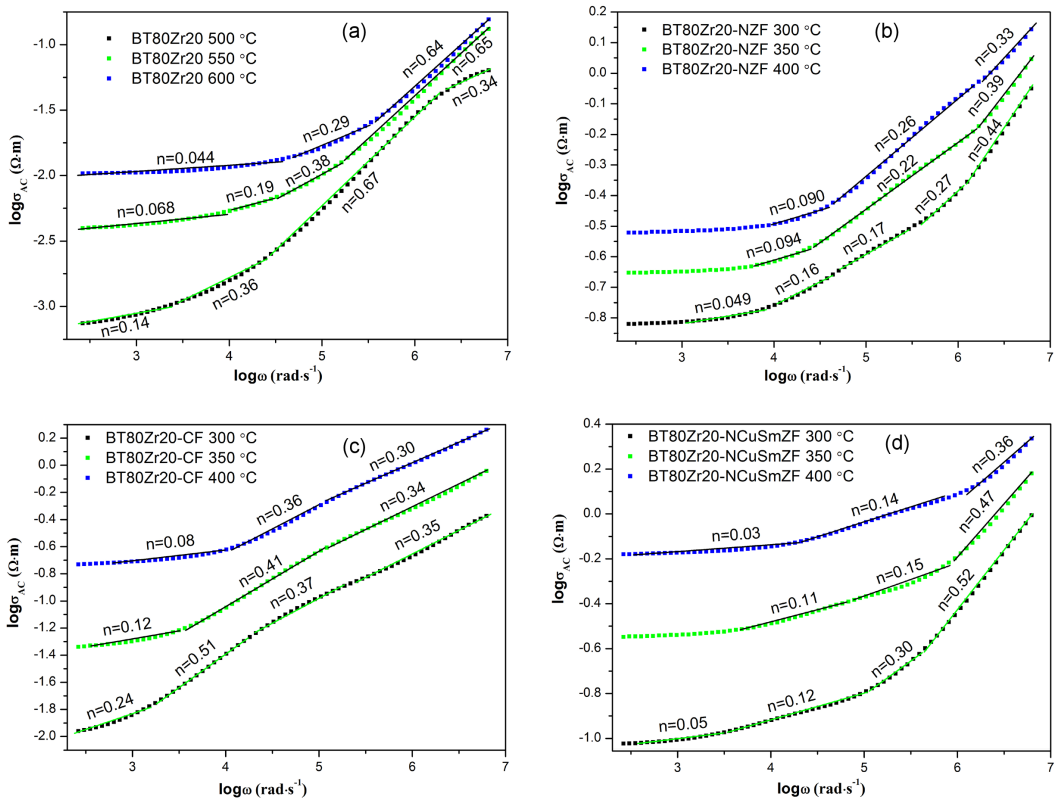

Figure 10. Angular frequency dependence AC conductivity of: a) BT80Zr20, b) BT80Zr20-NZF, c) BT80Zr20-CF and d) BT80Zr20-NCuSmZF at different temperatures

not the case for other two composites, in which there was no presence of expressed peaks expected at higher frequencies.

In general, the existence of peaks in the low frequency region suggests the movement of ions over the long distances, whereas the appearance of high frequency peaks suggests the confinement of ions in their potential well [41]. In this study, in the pure BZrT ceramics, the presented modulus spectrum indicated possible movement of charge carriers (ions and defects) at both long and short distances. However, the situation in the composites is pretty different. The BT80Zr20-CF ceramics have shown peaks at higher frequencies, indicating possible movement of electrical charge only over the short distances. For the other two composites, containing NF and NZCuSmF, a hardly noticeable anomaly can be found at lower frequencies and no peaks up to 1 MHz. There is also the existing possibility that these peaks will appear at much higher frequencies, since in the composites with CF the movement of the curves' maximum to higher frequency side is evident. Obviously, the asymmetry in peaks broadening for all ceramics can be noticed, proposing the non-Debye type of relaxation [41].

In order to confirm which type of polarons determines the conduction, we have investigated AC conductivity using the equation $\sigma_{AC}(\omega) = \varepsilon_0 \cdot \varepsilon'' \cdot \omega$, where ε_0 is the permittivity of the free space, ε'' is imaginary part of the dielectric permittivity and ω is angular frequency as a function of frequency at different temperatures. Figure 10 represents logarithmic dependence of AC conductivity on angular frequency in the temperature range 500–600 °C for the BT80Zr20 and 300–400 °C for all three composites materials.

In the low frequency region there is apperently frequency independent plateau explained by the jump relaxation model where the conduction is probably happening trough the hopping of charged particles from one localized state to another [42]. In the higher frequency region, AC conductivity is dependent on the frequency and obviously obeys the Jonscher power low [43]:

$$\sigma(\omega) = \sigma(0) + A(T)\omega^n \qquad (2)$$

where $\sigma(\omega)$ is total conductivity, $\sigma(0)$ is DC conductivity while $A(T)$ and n are temperature and materials intrinsic property dependent constant, respectively. From the slopes of these curves, the values of exponent n can be obtained. Value of n for all composite samples was found to be between 0 and 0.5. According to the literature data for a majority of disordered solids [44] these values can be attributed to the ionic hopping that occurs in grains. However, for the BT80Zr20 ceramics in the high frequency region this value is between 0.5 and 1 and it can be attributed to the ionic hopping in the grain and grain boundary regions [45]. Many conductivity mechanisms in materials can be understood from the combination of the temperature dependent behaviour of n and frequency dependent behaviour of n [46,47]. In the case where the exponent n depends on the frequency but it is temperature independent the quantum mechanical tunnelling model (QMT) can be proposed, and the conductivity is attributed to the phonon-assisted tunnelling between defect states. If the exponent n simultaneously depends on the temperature and frequency, then the overlapping large-polaron tunnelling (OLPT) model can be acceptable, and in that case the tunnelling of polarons is the dominant mechanism. Peculiarly, if the exponent n decreases with temperature the correlated barrier hopping (CBH) model can be suggested. According to this model charge transport occurs between localized states due to the hopping over the potential barriers. In this study, for all composites, there is a trend of decreasing value of exponent n with temperature and it is also frequency dependent which indicates the presence of CBH model of conduction in material. The value of exponent n in the BT80Zr20 is both frequency and temperature dependent proposing the OLPT model of conduction in the material.

The value of DC conductivity can be determined by extrapolation of AC conductivity at low frequencies. This value was used to obtain values of activation energies (Fig. 11) for the conduction processes in the materials from the Arrhenius low: $\sigma_{DC} = \sigma_0 \cdot \exp(-E_{DC}/kT)$. The values of activation energies obtained from the slopes of the curves (Fig. 11) correspond to the value of activation energy obtained from the impedance measurements. The value of activation energy for the BT80Zr20 (1.54 eV) indicated the presence of intrinsic defects-migration of oxygen vacancies and conductivity in this material correspond to the mobility of the defects in the crystal lattice. These values of activation energy differ from the ones obtained for the investigated composites, indicating the influence of different ferrites in the composites on the conductivity of material. The composite BT80Zr20-NZF had the value of activation energy close to 0.2 eV - suggesting

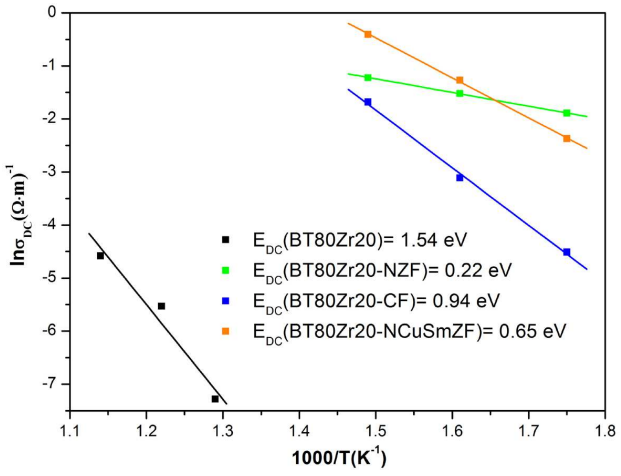

Figure 11. The Arrhenius plots of DC conductivity for BT80Zr20, BT80Zr20-NZF, BT80Zr20-CF and BT80Zr20-NCuSmZF ceramics

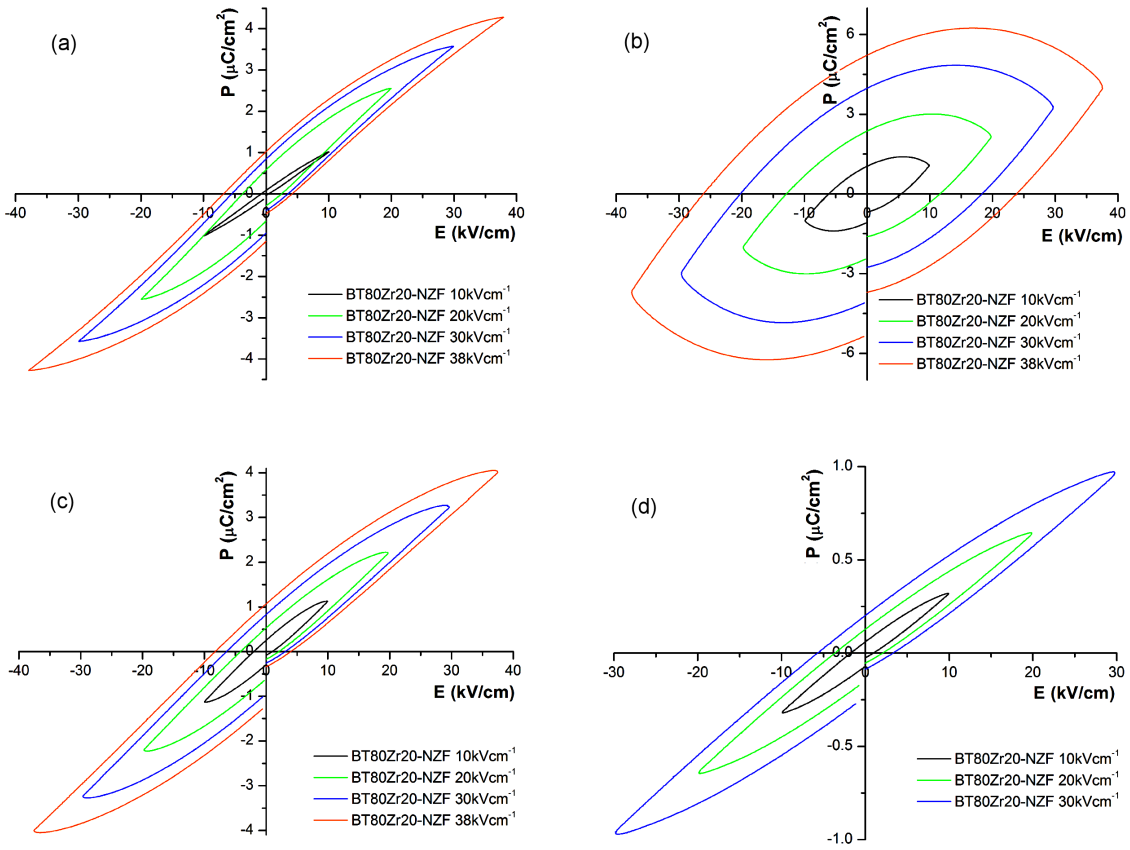

Figure 12. Hysteresis *P-E* loops for all investigated samples

two types of polaronic conduction, polaronic conduction of the holes and n-type polaronic conduction. For the BT80Zr20-CF mobility of the defects in the crystal lattice may be considered as a type of dominant conduction, while in the BT80Zr20-NCuSmZF, where the energy of activation is above 0.2 eV, the polaronic conduction of the holes can be proposed [48,49].

The polarization vs. electric field measurements at room temperature were performed by applying the electrical field in the range of 10–38 kV/cm (Fig. 12). Typical hysteresis loops for ferroelectric materials were obtained for the pure BT80Zr20 ceramics. In the composites, the addition of ferromagnetic phase with higher conductivity influences the ferroelectric order in the materials, therefore the shape of these curves differs from the conventional ferroelectric materials and it is obviously influenced by the properties of magnetic phase [50]. Since the obtained loops are not well saturated it is very difficult to determine remnant polarization and coercive field with high accuracy. The sample BT80Zr20-NZF possesses the higher value of E_c in comparison to the BT80Zr20-CF and BT80Zr20-NCuSmZF. The reason for that can be the presence of the large number of oxygen vacancies which may originate from the sintering process in the air where the oxygen loss during the sintering can produce oxygen vacancies but also from Ti^{4+}, which can easily be reduced to Ti^{3+} which leads to the formation of oxygen vacancies. Also, these composites possess higher value of E_c in comparison with the BT80Zr20 because the composites are more difficult to be polarized and the movement of the domains is limited [51,52]. The BT80Zr20-CF and BT80Zr20-NCuSmZF ceramics have shown slightly deteriorated ferroelectric loops in comparison with the pure BZrT ceramics but composite with NZF have shown pretty lossy nature. This is in accordance with the fact that NZF is the most conductive magnetic phase used for the composites in this study. The possible explanation could be intensive pinning or clamping of ferroelectric domains by ferromagnetic NZF, which acts as an obstacle for the domain wall motion in this type of composites.

It is difficult to explain which ferrite phase has the greatest impact on ferroelectric properties because none of the materials did not reach the saturation. It seems that the BT80Zr20-CF, if saturated, would have the highest value of P_r and P_s, which makes this material potentially the most suitable for the ferroelectric application.

The leakage current density (j) was measured at room temperature as a function of static electric field (E) for the BT80Zr20 and BT80Zr20-NZF, BT80Zr20-CF, BT80Zr20-NCuSmZF composites in order to further study conductivity mechanisms in these materials. BT80Zr20-NZF possessed the highest value of leakage current density of all the investigated composites and the lowest was for the BT80Zr20-NCuSmZF. This is related to the fact that the BT80Zr20-NZF possesses the lowest resistivity among the investigated compos-

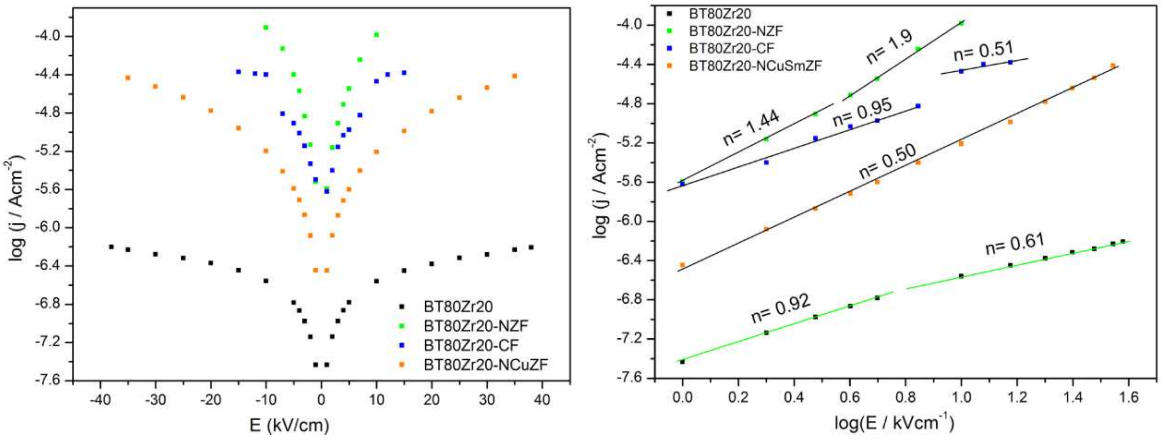

Figure 13. Leakage measurements as: a) log*j*-*E* dependence and b) log*j*-log*E* dependence

ites. The BT80Zr20 possesses a lower leakage current density compared to composites, which was expected due to the high resistance of the BT80Zr20 [53]. The log *j*-log *E* dependence is presented in Fig. 13. The obtained lines were well fitted by the power low $j \sim E^n$, where n is the slope of the linear part of the curve in the log-log plots used for the determination of the conduction nature in the materials. According to the n value, there are four possible mechanisms of conduction: grain boundary limited conduction (GBLC), ohmic conduction mechanism, space charge limited conduction (SCLC) or trap-controlled SCLC mechanism. The BT80Zr20 ceramics, in low field region, has the value of n between 1 and 1.5 which suggests the existence of Ohmic conduction mechanism [54]. This mechanism is characterized by the thermally generated free carriers density being higher than the density of injected charge carriers. In the high field region, this value is between 1.5 and 2 which pointed to the existence of space charge limited conduction. This mechanism presumes the injected charge carriers as dominant. For the composites samples, in both field regions, the value of n is less than 1 suggesting the grain boundary limited conduction. These results are in accordance with the presented impedance analysis in which it was seen that the resistivity of the grain boundaries is significantly higher in comparison with the resistivity of the grains. Thus, especially in the composites, the conduction could be limited mainly by the electrical properties determined by the grain boundaries [54].

IV. Conclusions

In summary, composites were successfully formed by the mixing of the previously auto-combustion-synthesized NZF, CF, NCuSmZF and BT80Zr20 magnetic-ferroelectric ceramic powders. SEM results showed the existence of the two distinct phases, ferrite and ferroelectric phases, with the average grain size from 0.7–1.5 μm. The impedance results have shown differences between the pure ferroelectric and composite materials and the temperature dependent electrical relaxation in material. The value of calculated activation energy indicated the presence of conduction which corresponds to the mobility of the defects in the crystal lattice for the BT80Zr20 and BT80Zr20-CF while for other two composites electron hopping conduction is recommended. *P-E* hysteresis loops showed non-saturated loops where the composites possess higher value of E_c in comparison with the BT80Zr20 because they are more difficult to be polarized and movement of the domains is limited. Investigation of AC and DC conductivities confirmed the presence of two regions of conduction: frequency independent region which can be explained by the jump relaxation model at low frequencies and frequency dependent region at high frequencies which obeys the Jonscher power low. Leakage current density measurements suggested the change of the conduction mechanism from SCLC to ohmic type where the BT80Zr20 possesses a lower leakage current density compared to the composites.

Acknowledgements: The authors gratefully acknowledge the Ministry of Education, Science and Technological Development Republic of Serbia to financial support given through national programs (project code 451-03-68/2020-14/200053).

References

1. S. Upadhyay, V. Reddy, N. Lakshmi, "Study of (1-x) $BaTiO_3$-x$Ni_{0.5}Zn_{0.5}Fe_2O_4$ (x = 5, 10 and 15%) magneto-electric ceramic composites", *J. Asian. Ceram. Soc.*, **1** (2013) 346–350.
2. M. Bibes, A. Barthelemy, "Towards a magnetoelectric memory", *Nat. Mater.*, **7** (2008) 425–426.
3. H. Palneedi, V. Annapureddy, S. Priya, J. Ryu, "Status and perspectives of multifferoic magnetoelectric composite materials and application", *Actuators*, **5** (2016) 9.
4. W. Prellier, M. Singh, P. Murugavel, "The single-phase multiferroic oxides: From bulk to thin film", *J. Phys. Condens. Matter*, **17** (2005) R803–R832.
5. G. Catalan, J. Scott, "Physics and applications of bismuth ferrite", *Adv. Mater.*, **21** (24) (2009) 2463–2485.
6. T. Zhao, A. Scholl, F. Zavaliche, K. Lee, M. Barry, A. Doran, M. Cruz, Z. Chu, C. Ederer, N. Spaldin, R. Das, D.

Kim, S. Baek, C. Eom, R. Ramesh, "Electrical control of antiferromagnetic domains in multiferroic $BiFeO_3$ films at room temperature", *Nat. Mater.*, **5** [10] (2006) 823–829.
7. P. Anantharamaiah, P. Joy, "Enhancing the strain sensitivity of $CoFe_2O_4$ at low magnetic fields without affecting the magnetostriction coefficient by substitution of small amounts of Mg for Fe", *Phys. Chem. Chem. Phys.*, **18** [15] (2016) 10516–10527.
8. M. Bichurin, V. Petrov, G. Srinivasan, "Theory of low-frequency magnetoelectric effects in ferromagnetic-ferroelectric layered composites", *J. Appl. Phys.*, **92** [12] (2002) 7681–7683.
9. C. Nan, "Magnetoelectric effect in composites of piezoelectric and piezomagnetic phases", *Phys. Rev. B*, **50** [9] (1994) 6082–6088.
10. A. Dzunuzovic, M. Vijatovic Petrovic, B. Stojadinovic, N. Ilic, J. Bobic, C. Foschini, M. Zaghete, B. Stojanovic, "Multiferroic (NiZn)Fe_2O_4-$BaTiO_3$ composites prepared from nanopowders by auto-combustion method", *Ceram. Int.*, **41** (2015) 13189–13200.
11. M. Vijatovic Petrovic, R. Grigalaitis, A. Dzunuzovic, J. Bobic, B. Stojanovic, R. Salasevicius, J. Banys, "Positive influence of Sb doping on properties of di-phase multiferroics based on barium titanate and nickel ferrite", *J. Alloy. Compd.*, **749** (2018) 1043–1053.
12. A. Dzunuzovic, M. Vijatovic Petrovic, J. Bobic, N. Ilic, M. Ivanov, R. Grigalaitis, J. Banys, B. Stojanovic, "Magnetoelectric properties of $xNi_{0.7}Zn_{0.3}Fe_2O_4$-(1-x)$BaTiO_3$ multiferroic composites", *Ceram. Int.*, **44** (2018) 683–694.
13. J. Bobić, M. Ivanov, N. Ilić, A. Dzunuzović, M. Vijatović Petrović, J. Banys, A. Ribic, Z. Despotovic, B. Stojanovic, "PZT-nickel ferrite and PZT-cobalt ferrite comparative study: Structural, dielectric, ferroelectric and magnetic properties of composite ceramics", *Ceram. Int.*, **44** (2018) 6551–6557.
14. C. Ciomaga, C. Galassi, F. Prihor, I. Dumitru, L. Mitoseriu, A. Iordan, M. Airimioaei, M. Palamaru, "Preparation and properties of the $CoFe_2O_4$-Nb-Pb(Zr,Ti)O_3 multiferroic composites prepared in situ by gel-combustion method", *J. Alloy. Compd.*, **485** (2009) 372–378.
15. M. Selvaraj, R. Venkatesan, J. Mayandi, V. Venkatachalapathy, "Influence of tin(IV) doping on structural and optical properties of rhombohedral barium titanate ($BaTiO_3$)", *Mater. Today Proc.*, **35** (2021) 13–16.
16. R. Shi, Y. Pu, J. Ji, J. Li, X. Guo, W. Wang, M. Yang, "Correlation between flash sintering and dielectric breakdown behavior in donor-doped barium titanate ceramics", *Ceram. Int.*, **46** [8] (2020) 12846–12851.
17. V. Kavitha, J. Mayandi, P. Mahalingam, N. Sethupathi, "Structural, optical and electrical studies on zinc doped barium strontium titanate as photo-anode for DSSC device", *Mater. Today Proc.*, **35** (2021) 48–52.
18. N. Binhayeeniyi, P. Sukvisut, C. Thanachayanont, S. Muensit, "Physical and electromechanical properties of barium zirconium titanate synthesized at low-sintering temperature", *Mater. Lett.*, **64** (2010) 305–308.
19. Z. Yu, C. Ang, R. Guo, A. Bhalla, "Piezoelectric and strain properties of $Ba(Ti_{1-x}Zr_x)O_3$ ceramics", *J. Appl. Phys.*, **92** (2002) 1489–1493.
20. C. Nan, M. Bichurin, S. Dong, D. Viehland, G. Srinivasan, "Multi-ferroic magnetoelectric composites: historical perspective status and future directions", *J. Appl. Phys.*, **103** (2008) 031101.
21. N. Hosni, K. Zehani, T. Bartoli, L. Bessais, H. Maghraoui-Meherzi, "Semi-hard magnetic properties of nanoparticles of cobalt ferrite synthesized by the co-precipitation process", *J. Alloy. Compd.*, **694** (2017) 1295–1301.
22. V. Pissurlekar, "Magnetic and structural properties of $NiZnFe_2O_4$ ferrite nanopowders doped with Cu^{2+}", *Int. J. Sci. Res.*, **5** (2016) 1147–1149.
23. K. Batoo, M. Ansari, "Low temperature- fired Ni-Cu-Zn ferrite nanoparticles through auto-combustion method for multilayer chip inductor applications", *Nanoscale Res. Lett.*, **7** (2012) 112.
24. L. Li, L. Peng, X. Zhu, D. Yang, "Effect of Cu and Co substitution on the properties of NiZn ferrite thin films", *J. Electron. Sci. Technol.*, **10** (2012) 88–92.
25. M. Usakova, E. Usak, M. Soka, "Study of magnetic properties of samarium substituted nickel-zinc ferrite", *J. Electr. Eng.*, **66** (2015) 112–115.
26. V. Naidu, S. Ahamed, M. Dawood, M. Suganthi, "Magnetic properties of nano crystalline nickel, samarium doped zinc ferrite", *Int. J. Comp. Appl.*, **24** (2011) 18–22.
27. F. Weyland, T. Eisele, S. Steiner, T. Fromling, G. Roseti, J. Rodel, N. Novak, "Long term stability of electrocaloric response in barium zirzonate titanate", *J. Eur. Ceram. Soc.*, **38** [2] (2018) 551–556.
28. M.M. Vijatovic Petrovic, A. Dzunuzovic, J.D. Bobic, N. Ilic, I. Stijepovic, B.D. Stojanovic, "Study of barium titanate/nickel-zinc ferrite based composites: Electrical and magnetic properties and humidity sensitivity", *Process. Appl. Ceram.*, **14** [1] (2020) 9–18.
29. B. Suryanarayana, K. Chandra Mouli, V. Raghavendra, B.B. Parvateesam, "Synthesis and magnetic studies of Ni-Cu-Zn ferrite nanocrystals", *National Conference on Advanced Functional Materials and Computer Applications in Materials Technology* (CAMCAT-2014).
30. L. Gama, A. Diniz, A. Costa, S. Rezende, A. Azevedo, D. Cornejo, "Magnetic properties of crystalline Ni-Zn ferrites doped with samarium", *Physics B*, **384** (2006) 97–99.
31. V. Awati, "Synthesis and characterization of Ni-Cu-Zn ferrite materials by auto combustion technique", *Int. J. Chem. Phys. Sci.*, **4** (2015) 50–59.
32. W. Warren, K. Vanheusden, D. Dimos, G. Pike, B. Tuttle, "Oxygen vacancy motion in perovskite oxides", *J. Am. Ceram. Soc.*, **79** [2] (1996) 536–538.
33. A. Muller, H. Hardtl, "Ambipolar diffusion phenomena in $BaTiO_3$ and $SrTiO_3$", *Appl. Phys. A*, **49** (1989) 75–82.
34. J. Rodel, G. Tomandl, "Degradation of Mn-doped $BaTiO_3$ ceramic under a high d.c. electric field", *J. Mater. Sci.*, **19** [11] (1984) 3515–3523.
35. D. Cooper, C. Baeumer, N. Bernier, A. Marchewka, C. La Torre, R. Dunin-Borkowski, S. Menzel, R. Waser, R. Dittmann, "Anomalous resistance hysteresis in oxide ReRAM: Oxygen evolution and reincorporation revealed by in situ TEM", *Adv. Mater.*, **29** [23] (2017) 1700212.
36. M. Nobre, S. Lanfredi, "New evidence of grain boundary phenomenon in $Zn_7Sb_2O_{12}$ ceramic: An analysis by impedance spectroscopy", *Mater. Lett.*, **50** (2001) 322–327.
37. F. Kroger, H. Vink, "Relations between the concentrations of imperfections in crystalline solids", *Solid State Phys.*, **3** (1956) 307.
38. S. Brahma, R. Choudhary, A. Thakur, "AC impedance analysis of $LaLiMo_2O_8$ electroceramics", *Physica B*, **355** (2005) 188–201.

39. P. Kumar, S. Singh, M. Spah, J. Juneja, C. Prekash, K. Raina, "Synthesis and dielectric properties of substituted barium titanate ceramics", *J. Alloy. Compd.*, **489** (2010) 59–63.
40. B. Behera, P. Nayak, R. Choudhary, "Structural and impedance properties of $KBa_2V_5O_{15}$ ceramics", *Mater. Res. Bull.*, **43** (2008) 401–410.
41. M. Vijatovic Petrovic, R. Grigalaitis, N. Ilic, J. Bobic, A. Dzunuzovic, J. Banys, B. Stojanovic, "Interdependence between structure and electrical characteristics in Sm-doped barium titanate", *J. Alloy. Compd.*, **724** (2017) 959–968.
42. K. Funke, "Jump relaxation in solid electrolytes", *Prog. Solid State Chem.*, **22** (1993) 111–195.
43. K. Jonscher, "The 'universal' dielectric response", *Nature*, **267** (1977) 673–679.
44. S. Sen, S. K. Mishra, S. K. Das, A. Tarafdar, "Impedance analysis of $0.65Pb(Mg_{1/3}Nb_{2/3})O_3$-$0.35PbTiO_3$ ceramic", *J. Alloy. Compd.*, **453** (2008) 395–400.
45. S. Kumar, K. Varma, "Dielectric relaxation in bismuth layer-structured $BaBi_4Ti_4O_{15}$", *Curr. Appl. Phys.*, **11** (2011) 203–210.
46. B. Greenhoe, M. Hassan, J. Wiggins, K. Mauritz, "Universal power law behavior of the AC conductivity versus frequency of agglomerate morphologies in conductive carbon nanotube-reinforced epoxy networks", *J. Polym. Sci. B Pol. Phys.*, **54** (2016) 1918–1923.
47. V. Thakur, A. Singh, A.M. Awasthi, L. Singh, "Temperature dependent electrical transport characteristics of $BaTiO_3$ modified lithium borate glasses", *AIP Advances*, **5** (2015) 087110.
48. Y. Wu, M. Forbess, S. Seraji, S. Limmer, T. Chou, C. Nguyen, G. Cao, "Doping effect in layer structured $SrBi_2Nb_2O_9$ ferroelectrics", *J. Appl. Phys.*, **90** (2001) 5296–5303.
49. Y. Wu, G. Cao, "Ferroelectric and dielectric properties of strontium bismuth niobate vanadates", *J. Mater. Res.*, **15** (2000) 1583–1590.
50. L. Bai, R. Gao, Q. Zhang, Z. Xu, Z. Wang, C. Fu, G. Chen, X. Deng, W. Cai, "Influence of molar ratio on dielectric, ferroelectric and magnetic properties of $Co_{0.5}Mg_{0.5}Fe_2O_4/Ba_{0.85}Sr_{0.15}TiO_3$ composite ceramics", *Process. Appl. Ceram.*, **13** [3] (2019) 257–268.
51. M. Dawber, K. Rabe, J. Scott, "Physics of thin-film ferroelectric oxide", *Rev. Modern Phys.*, **77** (2005) 1084–1130.
52. N. Kitamura, T. Mizoguchi, T. Itoh, Y. Idemoto, "Ferroelectric performances and crystals structures of $(Pb,La)(Zr,Ti,Nb)O_3$", *J. Solid State Chem.*, **210** (2014) 275–279.
53. X. Luo, H. Wang, R. Gao, X. Li, J. Zhang, H. Ban, "Effects of molar ratio on dielectric, ferroelectric and magnetic properties of $Ni_{0.5}Zn_{0.5}Fe_2O_4$-$BaTiO_3$ composite ceramics", *Process. Appl. Ceram.*, **14** [2] (2020) 91–101.
54. F.C. Chiu, "A review on conduction mechanisms in dielectric films", *Adv. Mater. Sci. Eng.*, **2014** (2014) 578168.